AMERICAN SOCIETY FOR MICROBIOLOGY | Applied and Environmental Microbiology®

BIODEGRADATION

Insights into the Function and Horizontal Transfer of Isoproturon Degradation Genes (*pdmAB*) in a Biobed System

Veronika Storck,[a] Sara Gallego,[a] Sotirios Vasileiadis,[b] Sabir Hussain,[c] Jérémie Béguet,[a] Nadine Rouard,[a] Céline Baguelin,[b,d] Chiara Perruchon,[b] Marion Devers-Lamrani,[a] Dimitrios G. Karpouzas,[b] Fabrice Martin-Laurent[a]

[a]Agroécologie, AgroSup Dijon, INRAE, Université Bourgogne, Université Bourgogne Franche-Comté, Dijon, France
[b]University of Thessaly, Department of Biochemistry and Biotechnology, Laboratory of Plant and Environmental Biotechnology, Viopolis, Larisa, Greece
[c]Department of Environmental Sciences and Engineering, Government College, University of Faisalabad, Faisalabad, Pakistan
[d]Hydreka Enoveo, Lyon, France

Veronika Storck (microcosm experiment 1), Sara Gallego (microcosm experiment 2), and Sotirios Vasileiadis (microcosm experiment 3) contributed equally to this work and agreed on the order of their names.

ABSTRACT Biobeds, designed to minimize pesticide point source contamination, rely mainly on biodegradation processes. We studied the interactions of a biobed microbial community with the herbicide isoproturon (IPU) to explore the role of the *pdmA* gene, encoding the large subunit of an *N*-demethylase responsible for the initial demethylation of IPU, via quantitative PCR (qPCR) and reverse transcription-PCR (RT-qPCR) and the effect of IPU on the diversity of the total bacterial community and its active fraction through amplicon sequencing of DNA and RNA, respectively. We further investigated the localization and dispersal mechanisms of *pdmAB* in the biobed packing material by measuring the abundance of the plasmid pSH (harboring *pdmAB*) of the IPU-degrading *Sphingomonas* sp. strain SH (previously isolated from the soil used in the biobed) compared with the abundance of the *pdmA* gene and metagenomic fosmid library screening. *pdmA* abundance and expression increased concomitantly with IPU mineralization, verifying its major role in IPU transformation in the biobed system. DNA- and RNA-based 16S rRNA gene sequencing analysis showed no effects on bacterial diversity. The *pdmAB*-harboring plasmid pSH showed a consistently lower abundance than *pdmA*, suggesting the localization of *pdmAB* in replicons other than pSH. Metagenomic analysis identified four *pdmAB*-carrying fosmids. In three of these fosmids, the *pdmAB* genes were organized in a well-conserved operon carried by sphingomonad plasmids with low synteny with pSH, while the fourth fosmid contained an incomplete *pdmAB* cassette localized in a genomic fragment of a *Rhodanobacter* strain. Further analysis suggested a potentially crucial role of IS*6* and IS*256* in the transposition and activation of the *pdmAB* operon.

IMPORTANCE Our study provides novel insights into the interactions of IPU with the bacterial community of biobed systems, reinforces the assumption of a transposable nature of IPU-degrading genes, and verifies that on-farm biobed systems are hot spots for the evolution of pesticide catabolic traits.

KEYWORDS *pdmAB*, isoproturon biodegradation, biobed, metagenomics, horizontal gene transfer

Pesticides are used in agriculture worldwide to protect crops from various pests and diseases. However, they can be harmful to the environment and human health (1). Point source contamination resulting from the uncontrolled environmental discharge of pesticide-contaminated agroindustrial effluents significantly contributes to the contamination of water resources by pesticides (2, 3). To cope with point source contamination, a simple biopurification system called biobed was developed (4) and used

Citation Storck V, Gallego S, Vasileiadis S, Hussain S, Béguet J, Rouard N, Baguelin C, Perruchon C, Devers-Lamrani M, Karpouzas DG, Martin-Laurent F. 2020. Insights into the function and horizontal transfer of isoproturon degradation genes (*pdmAB*) in a biobed system. Appl Environ Microbiol 86:e00474-20. https://doi.org/10.1128/AEM.00474-20.

Editor Hideaki Nojiri, University of Tokyo

Address correspondence to Fabrice Martin-Laurent, fabrice.martin@inrae.fr.

Received 24 February 2020
Accepted 30 April 2020
Accepted manuscript posted online 15 May 2020
Published 2 July 2020

in various formats to treat effluents produced by on-farm activities (5, 6) or fruit-packaging plants (7). In its typical form, a biobed is a pit on the ground packed with bioorganic material composed of soil, straw, and peat or compost mixed at various volumetric ratios (2). This packing material supports an active microbial community able to degrade a wide range of pesticides, playing a key role in the efficiency of biobed systems (8).

To the best of our knowledge, only a few studies have explored the composition (9, 10) and functions (11) of microbial communities in biobed systems. Repeated exposure to high pesticide loads leads to the proliferation of bacterial populations able to rapidly degrade pesticides and to use them as a nutrient source, as shown in biobeds for linuron-degrading bacteria carrying the hydrolase-encoding genes *hylA* and *libA* (12). The growth of specific pesticide-degrading microbial guilds can be monitored by measuring the abundance and expression of pesticide-specific catabolic genes, as was done in previous soil studies (13–16). However, this approach does not provide any taxonomic information on the microbial degraders. To this end, advanced amplicon sequencing methods can be suitable to identify microorganisms growing at the expense of pesticides. As such, Itoh et al. observed a gradual increase in the abundance of *Burkholderia* bacteria in a soil repeatedly treated with fenitrothion and proposed their involvement in the degradation of this compound (17). Using an RNA-based analysis, Gallego et al. observed limited changes in the composition of the bacterial community in response to oxamyl applications in soil exhibiting an enhanced biodegradation of oxamyl (18). Previous studies have used different high-throughput approaches, such as taxon-specific quantitative PCR (qPCR) (19) and amplicon sequencing (20, 21), to define the responses of the microbial communities to pesticide applications in agricultural soils but not yet in biobed systems exposed to high pesticide loads.

Gu et al. identified the bacterial genes *pdmAB*, encoding the oxygenase components of an *N*-demethylase, as being responsible for the biodegradation of the phenylurea herbicide isoproturon (IPU) in soil (22). However, no information is available regarding their occurrence, distribution, and activity in biobed systems, where effluents containing IPU are regularly discharged. PdmAB catalyzes the first and key step in the bacterial transformation of IPU, its N-demethylation to monodemethyl-IPU (MD-IPU) and didemethyl-IPU (DD-IPU) (23). The demethylated IPU products are transformed into 4-isopropylo-aniline (4-IA) by a DdhA hydrolase. 4-IA is further converted by aniline dioxygenase (*ado*, *tdn*, and *atd* genes) to catechol and finally transformed into C_1 compounds through the relevant *ortho* or *meta* cleavage pathway (23) (see Fig. S1 in the supplemental material). The *pdmAB* genes were detected in several IPU-degrading bacterial strains, such as *Sphingobium* sp. strain YBL2, isolated from soil in China (GenBank accession number CP010958.1); *Sphingomonas* sp. strain SRS2, isolated from soil in the United Kingdom (GenBank accession number LARW01000036.1); and *Sphingomonas* sp. strain SH, isolated from the soil of the experimental farm of INRAE, Dijon, France (22, 24, 25). Interestingly, in all these strains, the *pdmAB* genes were located in a conserved cassette, which comprised, apart from *pdmAB*, two genes encoding a glyoxylase family protein and a *cis*-2,3-dihydrobiphenyl-2,3-diol dehydrogenase (23). This cassette resides mostly in plasmids such as pSH (GenBank accession number KU237244.1) (Fig. S2) of *Sphingomonas* sp. SH and YBL2-p4 of *Sphingobium* sp. YBL2. Besides *pdmAB*, pSH carries *ddhA*, responsible for the cleavage of the urea side chains of MD-IPU and DD-IPU, but no aniline dioxygenase or a catechol cleavage operon, unlike *Sphingobium* YBL2, which has the *pdmAB*, *ddhA*, and aniline dioxygenase genes localized in three different plasmids (23). This genetic organization of *pdmAB* implies that horizontal gene transfer controls their dispersal in the bacterial community, although direct evidence for this is still lacking. Previous studies showed that biobeds are enriched in mobile genetic elements (MGEs) (26, 27), providing the first evidence of their key role in the dispersal of biodegradation-related traits within the bacterial community of biobed systems. However, the identity of the holders of these MGEs, their localization in the metagenome or plasmidome of biobeds, and their functional role in the degradation of IPU remain unexplored.

In this context, the aims of this study were (i) to explore the role of the *pdmA* microbial guild in the mineralization of IPU in a biobed packing material, (ii) to investigate the response of the overall bacterial community of the biobed packing material to IPU and identify (positively or negatively) affected members, and (iii) to obtain insights into the evolution, localization, and possible dispersal mechanism of the *pdmAB* genes in a biobed system. Therefore, in a series of microcosm studies with biobed packing material collected from an operative biobed exposed to a range of pesticides, including phenylurea herbicides (Table S1), we (i) measured the mineralization of ^{14}C-ring-labeled IPU and correlated it with the abundance and expression of the *pdmA* gene and with the abundance of the *pdmAB*-containing plasmid pSH of the IPU-degrading *Sphingomonas* sp. strain SH (previously isolated from the soil used for the preparation of the biobed packing material), (ii) determined the composition of the total (DNA) and active (RNA) fractions of the bacterial community under IPU exposure by sequencing of 16S rRNA gene amplicons, and (iii) prepared and screened for the presence of *pdmA* in a fosmid metagenomic library from the biobed packing material and sequenced positive clones to provide insights into the localization and dispersal mechanisms of *pdmAB*.

RESULTS

Three independent microcosm experiments comprising triplicates for each treatment, schematically shown in Fig. 1, were employed to address the following main research questions of this study. What is the functional role of *pdmA* in the mineralization of IPU in a biobed system (microcosm experiments 1 and 2)? What is the response of the bacterial community of the biobed packing material to IPU exposure (microcosm experiment 2)? What are the localization and dispersal mechanisms of *pdmAB* driving its function in the biobed packing material (microcosm experiments 1 and 3)?

Microcosm experiment 1. In a first microcosm study (Fig. 1), we assessed the mineralization of ^{14}C-ring-labeled IPU and correlated it with the abundance of the *pdmA* gene. In parallel to the determination of the temporal dynamics of *pdmA* abundance, we monitored the dynamics of the plasmid pSH (see Fig. S2 in the supplemental material) carrying the *pdmAB* genes. A comparison of its abundance to that of the IPU-degrading genes can indicate if they are cargo of only pSH or if they are carried by other replicons.

(i) IPU mineralization. IPU was readily mineralized in the biobed packing material, with half of the initially applied ^{14}C-ring-labeled IPU evolving as $^{14}CO_2$ within 2 weeks (Fig. 2). IPU mineralization followed first-order kinetics, with a maximum IPU mineralization (A) of 53.6% $\pm$ 0.4% (yield expressed as a percentage of the initially added radioactivity), a maximum mineralization rate (μ_m) of 12.8% $\pm$ 0.6% per day, and a lag phase (λ) of 1.6 $\pm$ 0.0 days, as calculated by fitting the modified Gompertz growth model to the IPU mineralization curve.

(ii) *pdmA* and pSH abundances. A low number of copies of the *pdmA* gene was detected in the biobed packing material before IPU treatment (at 0 days, 22 copies per 10^4 copies of the 16S rRNA gene) (Fig. 2). Its relative abundance increased parallel to the mineralization of IPU, reaching its maximum level (262 $\pm$ 91 copies per 10^4 copies of the 16S rRNA gene) at day 7, which coincided with the end of the exponential phase of IPU mineralization (Fig. 2), and reverted to levels similar to those observed at 0 days at the end of the incubation period (at 14 days, 38 copies per 10^4 copies of the 16S rRNA gene [$P < 0.05$ by analysis of variance {ANOVA} followed by a Tukey test]). Parallel measurements of the relative abundance of the plasmid pSH, through the quantification of a pSH-specific sequence stretch (Fig. S2), showed a response pattern similar to that of the *pdmA* gene, although its abundance was significantly lower ($P < 0.05$ by ANOVA followed by a Tukey test) than that of *pdmA* throughout the incubation period (Fig. 2).

Microcosm experiment 2. A second microcosm study on the same biobed packing material was employed to (i) confirm the involvement of *pdmA* in the mineralization of IPU through measurement of its expression dynamics during the mineralization of

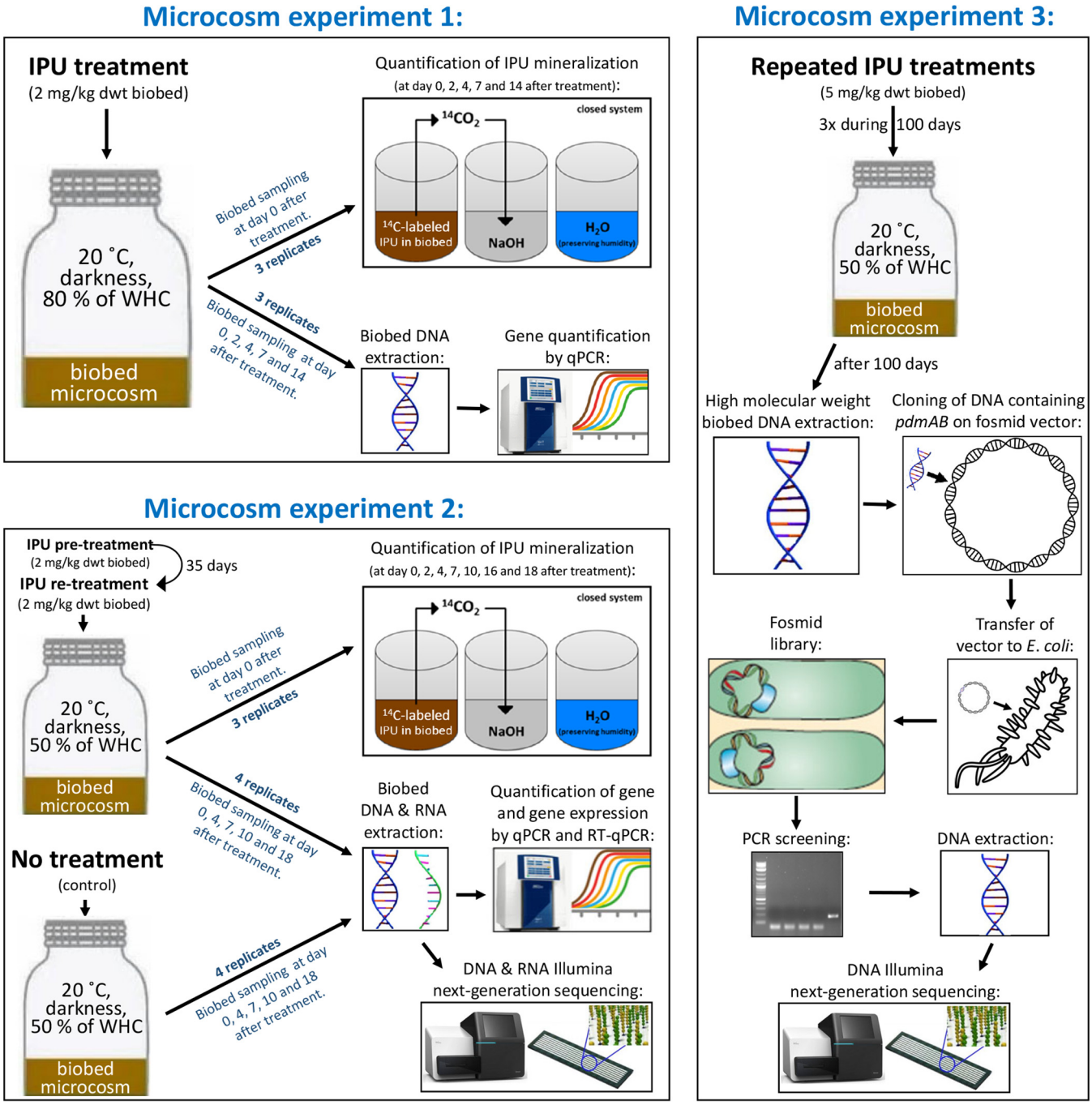

FIG 1 Schematic representation of the three microcosm experiments performed with the biobed packing material of the experimental farm of INRAE, Dijon, France, to determine (i) IPU mineralization and the abundance of the *pdmA* gene and the plasmid pSH (experiment 1); (ii) IPU mineralization, the abundance and expression of the *pdmA* gene, and the response of the total (DNA) and active (RNA) bacterial communities to IPU exposure (experiment 2); and (iii) the localization and genetic organization of the *pdmAB* genes in the indigenous bacterial community (experiment 3).

^{14}C-labeled IPU and (ii) explore the temporal responses of the total bacterial community and its active fraction to IPU exposure using DNA- and RNA-based amplicon sequencing of the 16S rRNA gene, respectively (Fig. 1). This can potentially lead to the identification of operational taxonomic units (OTUs) whose abundances increase (due to growth-linked biodegradation) or decrease (due to toxicity) in response to IPU exposure.

(i) IPU mineralization. In accordance with the first microcosm study, the mineralization of ^{14}C-labeled IPU in the second microcosm experiment followed first-order

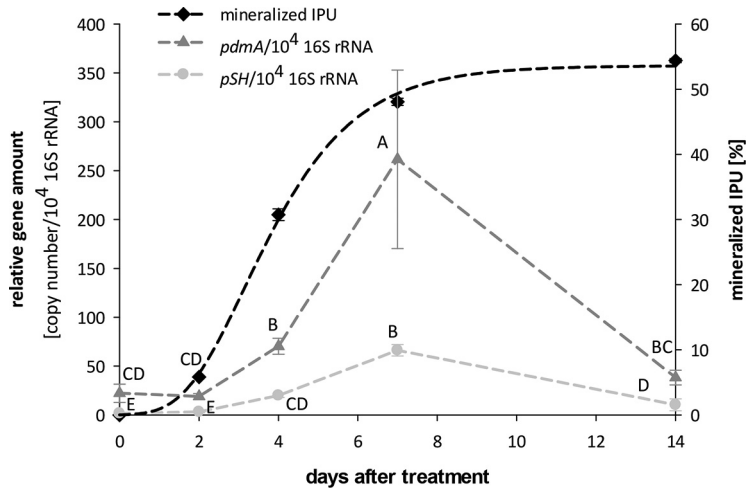

FIG 2 Microcosm experiment 1: mineralization pattern of ^{14}C-ring-labeled IPU (percentage of the initially applied ^{14}C) and relative abundances of the *pdmA* gene and plasmid pSH (copy number per 10^4 16S rRNA genes) in the biobed packing material. Values indicated by different letters are significantly different ($P < 0.05$ by ANOVA followed by a Tukey test).

kinetics, with a maximum *A* value of 49.1% ± 1.4%, a μ_m value of 4.2% ± 0.3% per day, and a λ value of 2.7 ± 0.2 days (Fig. 3a). Mass balance analysis performed at the end of the incubation period led to the recovery of 88.7% ± 2.4% of the initially added ^{14}C radioactivity (Fig. 3b). Only a small fraction of the initially applied ^{14}C radioactivity (1.7% ± 0.2%) was recovered in the extractable residue (ER) fraction, while a larger fraction of the initially added ^{14}C radioactivity (37.3% ± 0.9%) was retained by the biobed packing material and was recovered in the non-ER (NER) fraction (Fig. 3b).

(ii) Relative expression of the *pdmA* gene. The relative expression of the *pdmA* gene (ratio of the number of transcripts [RNA] to the number of copies [DNA]) was analyzed in biobed microcosms treated with a fresh IPU application and in control microcosms treated with water instead of IPU (Fig. 3a). At 0 days, transcripts of the

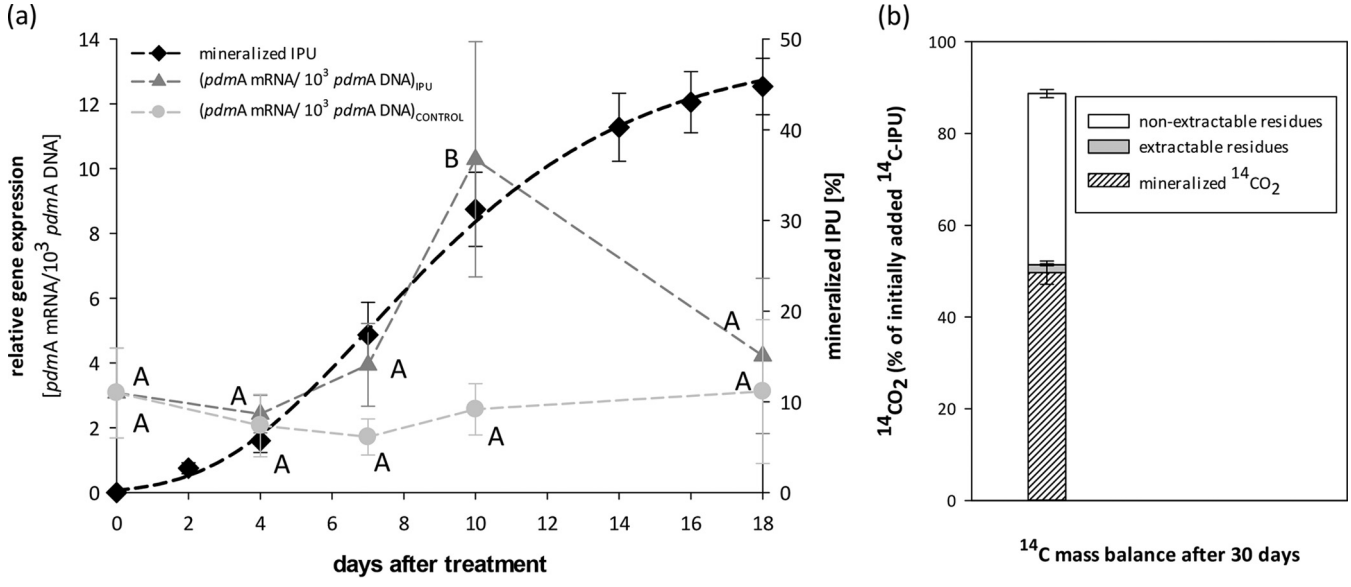

FIG 3 Microcosm experiment 2. (a) Mineralization pattern of ^{14}C-ring-labeled IPU (percentage of the initially applied ^{14}C) and relative expression of *pdmA* (ratio of the number of transcripts [RNA] to the number of copies [DNA]) in IPU-treated and untreated microcosms of the biobed packing material. Values indicated by different letters are significantly different ($P < 0.004$ by a Kruskal-Wallis test followed by a Conover-Iman test with a Bonferroni-corrected *P* value of 0.005). (b) Mass balance analysis of the ^{14}C-labeled residues in the biobed packing material.

pdmA gene were detected in both control and IPU-treated biobed packing material (3.07 ± 1.39 mRNA copies per 10^3 copies of DNA). In the treated samples, the relative expression of *pdmA* showed a significant increase ($P < 0.004$ by a Kruskal-Wallis test followed by a Conover-Iman test with a Bonferroni-corrected *P* value of 0.005) at day 10 (10.29 ± 3.63 mRNA copies per 10^3 copies of DNA) concomitantly with IPU mineralization. It then decreased to its initial levels by day 14. In contrast, the relative expression of *pdmA* did not significantly change during incubation in the control biobed packing material samples (Fig. 3a) ($P = 0.101$ by a Kruskal-Wallis test followed by a Conover-Iman test with a Bonferroni-corrected *P* value of 0.005). In fact, both *pdmA* expression and *pdmA* abundance remained at the initial levels in the control microcosms throughout the experiment (Table S2).

(iii) Impact of IPU on the diversity of the bacterial community in the biobed packing material. The effects of IPU on the diversity of the total bacterial community (DNA based) and its active fraction (RNA based) were determined by amplicon sequencing. In total, after demultiplexing and the removal of low-quality raw sequence reads, amplicon sequencing generated 6,468,787 high-quality 16S rRNA gene sequences with an average postassembly insert sequence length of 459 ± 13 bp. These sequences were grouped into 13,620 different OTUs, which were phylogenetically grouped (threshold of a 0.05% relative abundance) into 27 bacterial phyla (Fig. S3a). Regardless of treatment and time, *Proteobacteria* dominated both the total bacterial community and its active fraction, followed by *Actinobacteria*, *Acidobacteria*, *Verrucomicrobia*, and *Firmicutes* but at significantly lower abundances. Statistical analysis did not show any significant effects of IPU on the relative abundance of the dominant bacterial phyla ($P > 0.940$ by ANOVA followed by a Tukey test). Lower-taxonomic-level analysis showed no significant differences between treatments (IPU-treated and untreated samples) ($P > 0.013$ by a Kruskal-Wallis test followed by a Conover-Iman test with a Bonferroni-corrected *P* value of 0.0008) along the incubation time in the relative abundances of both the total and active fractions of the dominant bacterial orders (Fig. S3) and of the genera *Sphingomonas* (1,740 ± 155 sequences) and *Sphingobium* (2,706 ± 155 sequences) ($P > 0.200$ by a *t* test and a Welch test), expected to encompass IPU-degrading strains (Fig. S4). The Simpson reciprocal, Chao1, and phylogenetic diversity (PD) whole-tree α-diversity indices (Table S3) were not significantly affected by IPU exposure in both the total and the active fractions of the bacterial community ($P > 0.001$ for Simpson reciprocal diversity as determined by a Kruskal-Wallis test followed by a Conover-Iman test with a Bonferroni-corrected *P* value of 0.0008; $P > 0.052$ for Chao1 as determined by ANOVA followed by a Tukey test; $P > 0.003$ for the PD whole-tree index as determined by a Kruskal-Wallis test followed by a Conover-Iman test with a Bonferroni-corrected *P* value of 0.0008). Interestingly, Simpson reciprocal diversity indices were significantly higher for the active bacterial community than for the total bacterial community regardless of the treatment applied and the sampling time considered ($P < 0.0001$ by a Kruskal-Wallis test followed by a Conover-Iman test with a Bonferroni-corrected *P* value of 0.0008).

The potential impact of IPU on the β-diversity of the total bacterial community and its active fraction was explored by multivariate analysis. Principal-coordinate analysis (PCoA) from weighted UniFrac distance matrices between treatments (control versus IPU treated) and sampling times (7, 10, and 18 days) showed a clear separation of the total from the active bacterial community along PCoA axis 1, accounting for 90.7% of the variance (Fig. 4). Analysis of similarity (ANOSIM) followed by pairwise tests showed (i) significant time effects on the β-diversities of the total bacterial community in the control samples at day 10 and of the active fraction of the total bacterial community at days 7 and 10 compared to their respective compositions at day 0 (Table S4) and (ii) that IPU did not significantly affect the β-diversity ($P > 0.143$) of either the total or the active fraction of the bacterial community in the biobed packing material (Table S5).

Microcosm experiment 3: metagenomic analysis of the biobed packing material. A third microcosm experiment (Fig. 1) was employed to obtain insight into the localization, evolution, and dispersal mechanisms of the *pdmAB* genes through analysis

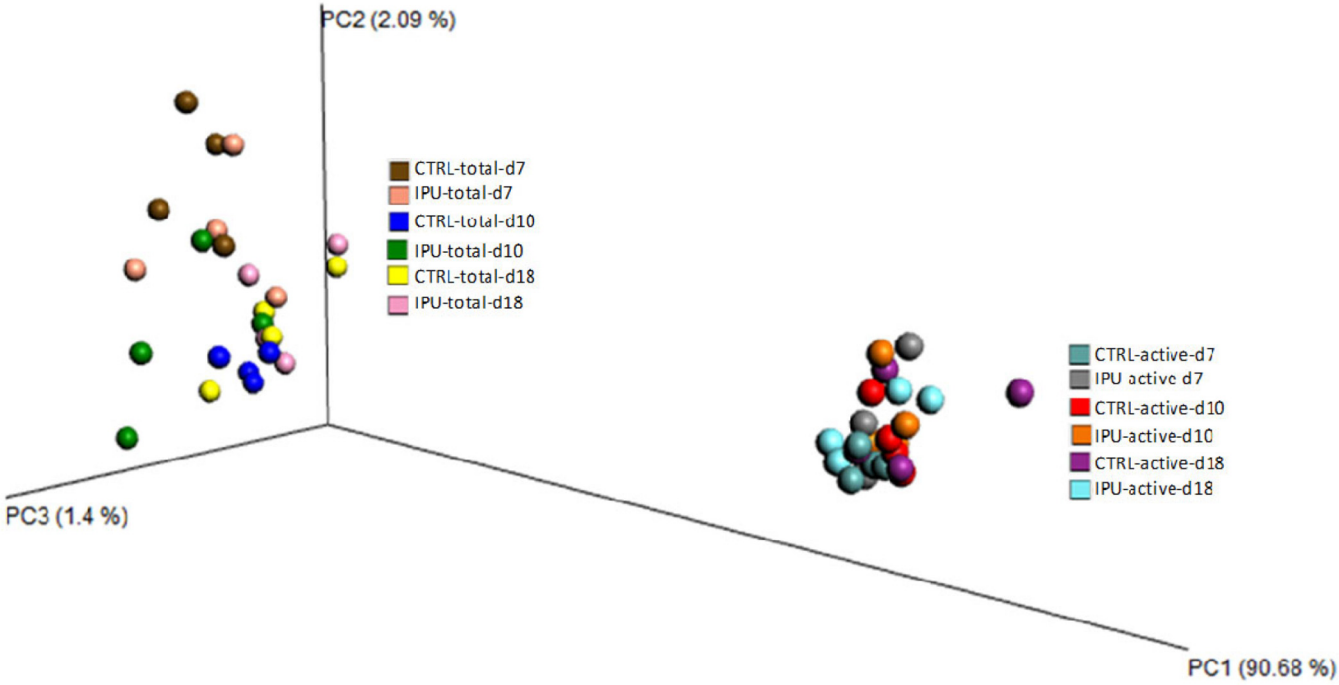

FIG 4 Microcosm experiment 2: PCoA on weighted UniFrac distance matrices based on the presence and absence of OTUs obtained by analysis of the total (DNA-based) and active (RNA-based) fractions of the bacterial community collected from the untreated (control [CTRL]) and IPU-treated (IPU) samples at day 7 (d7), day 10, and day 18. For each treatment, values from each of the four replicates are shown. Variance is expressed as a percentage on each axis.

of the metagenome of the bacterial community of the biobed material. In the first microcosm experiment, the pSH-specific sequence stretch was detected at a lower abundance than *pdmA*, implying that only a small fraction of the IPU-degrading bacterial community carried *pdmA* in pSH. We further pursued this through the preparation of a fosmid metagenomic library from DNA extracted from the biobed packing material. Its PCR screening led to the identification of four fosmids (fosmids 13, 14, 15, and 16) giving amplification of the *pdmA* gene. Sequencing of these fosmids generated inserts of 39.1, 34, 46.1, and 41.5 kb, which were assembled in a single contig, each containing 25, 27, 44, and 53 open reading frames (ORFs), respectively. The functional annotations of the detected ORFs are shown in Table S6. In fosmids 13, 15, and 16, *pdmAB* resided in a 4,460-bp cassette identical to the *pdmAB* cassettes of *Sphingomonas* sp. SH and *Sphingobium* sp. YBL2, being flanked by transposases belonging to different insertion sequence (IS) families and composed of genes encoding a glyoxalase dioxygenase, PdmA, PdmB, and a dihydrodiol dehydrogenase (Fig. 5). In contrast, fosmid 14 contained an incomplete *pdmAB* cassette, missing the gene coding for the dihydrodiol dehydrogenase, with mobile genetic elements (MGEs) found downstream of the *pdmAB* operon (Fig. 5). The *pdmAB* genes derived from the four fosmids and the *pdmAB* genes of the *Sphingomonas* sp. strain SH were 100% identical. We noted a single nucleotide difference of these sequences in comparison to the *pdmA* gene of *Sphingobium* sp. YBL2 (22). This single nucleotide difference resulted in a nonsilent amino acid change at position 309 (threonine versus alanine) of fosmid-derived PdmA.

Beyond the *pdmAB* region, the fosmids showed low overall synteny with plasmids pSH and YBL2-p4 (Fig. 6). The sole exception was fosmid 16, which showed synteny with pSH in a region of 8 kbp upstream of the *pdmAB* cassette encoding several hypothetical proteins, a plasmid partitioning protein (ParA), and mercury resistance proteins (MerT and MerR). Fosmids 13, 15, and 16 showed synteny with each other in a region encoding conjugation transfer proteins (*traACDG*). These fosmids also contained other genes of plasmid origin (*parAB*, *mobA*, and *virD*). In contrast, fosmid 14 showed no synteny with YBL2-p4, pSH, and the other three fosmids (except for the

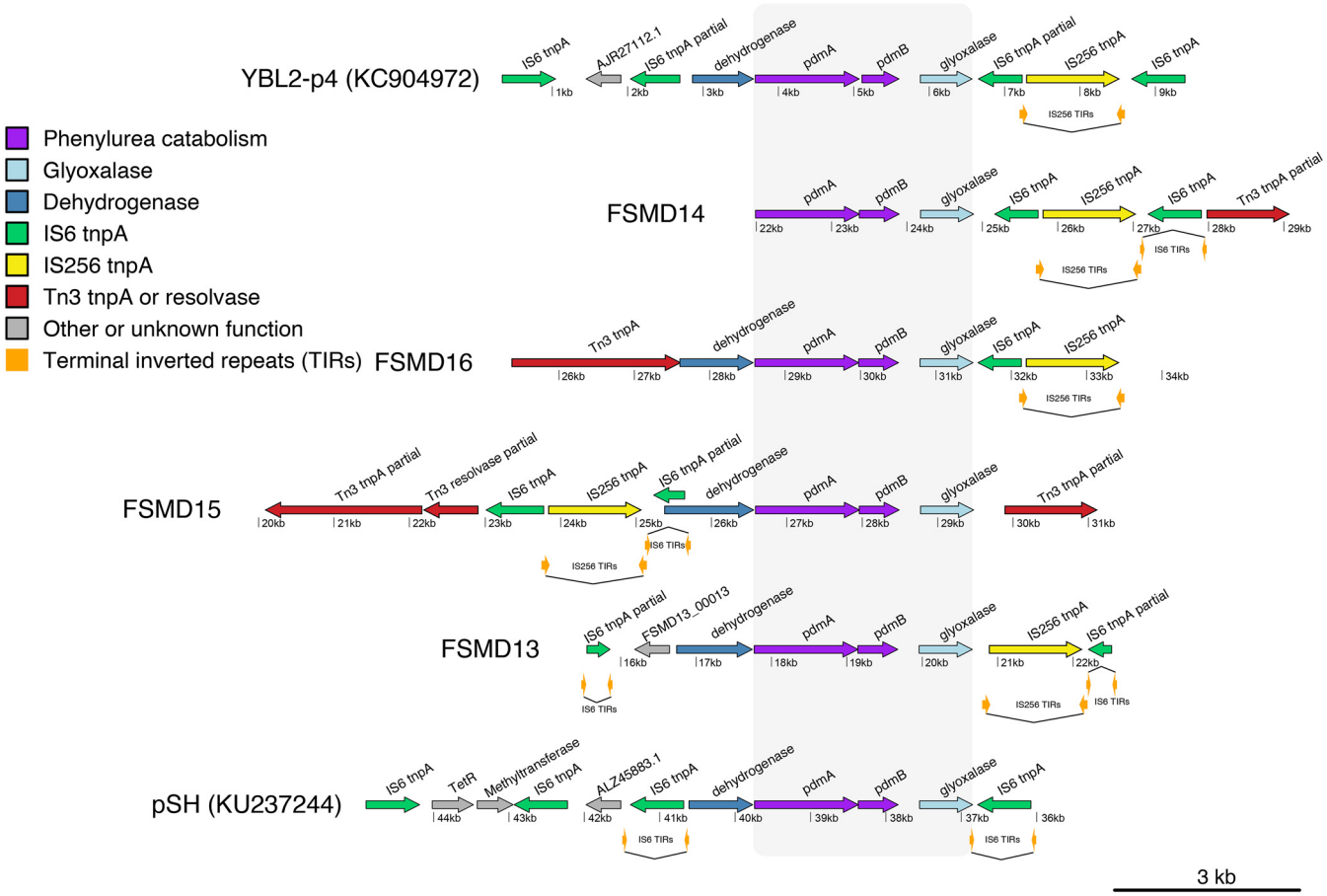

FIG 5 Microcosm experiment 3: organization of the genes in the *pdmAB* region in plasmids pSH of *Sphingomonas* sp. SH and YBL2-p4 of *Sphingobium* sp. YBL2 and in the four fosmids (FSMD13, -14, -15, and -16) derived from the metagenomic library of the biobed packing material. Different functional and phylogenetic annotations (regarding insertion sequences [IS]) of the genes are denoted with different colors, and terminal inverted repeats flanking mobile genetic elements (MGEs) are denoted with yellow arrows.

pdmAB region) (Fig. 6) and contained no plasmid-signatory genes (Table S6). Instead, it carried several housekeeping genes encoding enzymes involved in primary bacterial metabolism, such as (i) *aroE* participating in the biosynthesis of aromatic amino acids (28), (ii) *rpiB* involved in the pentose phosphate pathway (29), and (iii) *rimK* involved in

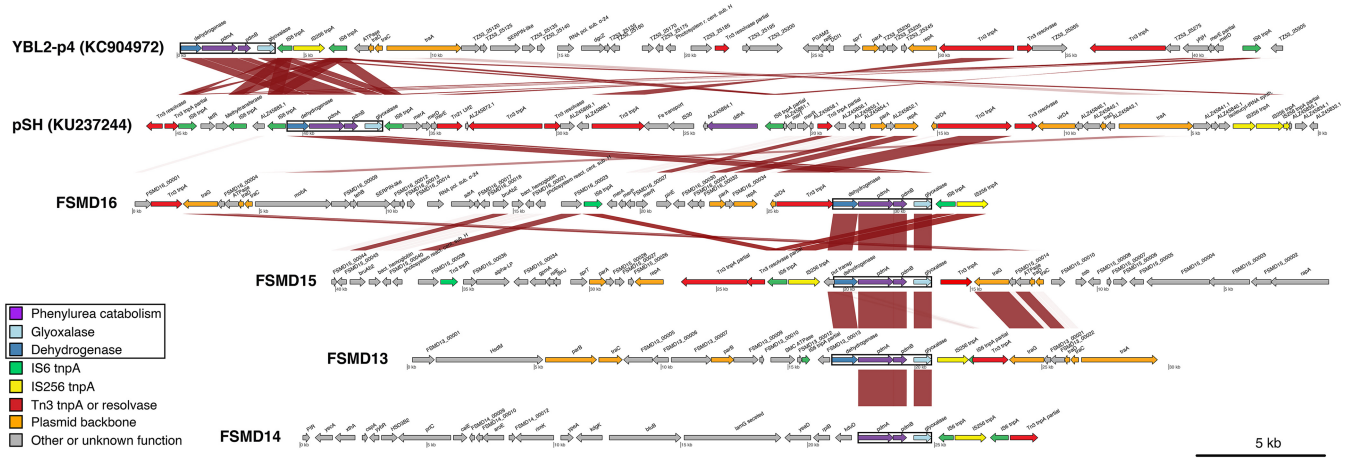

FIG 6 Microcosm experiment 3: synteny analysis of plasmid pSH of *Sphingomonas* sp. strain SH and plasmid YBL2-p4 of *Sphingobium* sp. YBL2 carrying the *pdmAB* cassette with the four fosmids (FSMD13, -14, -15, and -16) derived from the metagenomic library of the biobed packing material as positive for the presence of the *pdmAB* genes. Different functional annotations of the genes are denoted with different colors.

the biosynthesis of proteins (30), or in shock response mechanisms, such as *cspA* (31). All these ORFs were phylogenetically assigned to the family *Xanthomonadaceae* and especially to the genus *Rhodanobacter*. Finally, none of the fosmids carried the *ddhA* gene found in pSH (Fig. 6 and Table S6), known to be responsible for the cleavage of the urea side chains of MD-IPU and DD-IPU (23).

We expanded our analysis to the MGEs detected in the region of the *pdmAB* operon in fosmids compared to plasmids pSH and YBL2-p4. The phylogenetic annotations of MGEs in the fosmids/plasmids and associated terminal inverted repeats (TIRs) and direct repeats (DRs) are listed in Table S7, and their localization in the different replicons is presented in Fig. 5. In all fosmids and in YBL2-p4, the *pdmAB* cassette was flanked by MGEs belonging to the IS*6*, IS*256*, and Tn*3* families, compared to pSH, where the *pdmAB* cassette was flanked by only IS*6* family MGEs (Fig. 5). An alignment of the sequences of the IS*6* and IS*256* transposases flanking the *pdmAB* cassette showed that they were 100% identical in most cases (Table S8). In fosmids 14 and 16, the IS*6* element flanking the 3′ end of the *pdmAB* operon was truncated (576 bp of the 840-bp full length), most probably by a lateral insertion of a full-length IS*256* element (1,322 bp), which, unlike IS*6*, was flanked by 32-bp perfect TIRs and 9-bp DRs (Table S7). Fosmids 13 and 15 showed a different MGE localization pattern, whereby their *pdmAB* operon was directly flanked (on only one side) by IS*256* (always accompanied by 32-bp TIRs and 9-bp DRs), while truncated copies of IS*6* were found directly downstream. We further noticed several remnants of Tn*3* transposases (1,086 to 2,235 bp) in the region of the *pdmAB* operon of fosmids 13, 14, and 16, not accompanied by a resolvase. An exception was fosmid 15, where *tnpR* encoding a serine-type resolvase was found directly upstream of *tnpA* of the Tn*3* family (Table S6), in line with the typical composition of Tn*3* transposons (32). Unlike fosmids, the *pdmAB* operon in plasmids YBL2-p4 and pSH was flanked on both sides by IS*6*, forming a composite class I transposon, although in YBL2-p4, the copy of IS*6* found downstream of the *pdmAB* operon appears truncated, similarly to fosmids 14 and 16 (Fig. 5 and Table S7).

DISCUSSION

The biobed packing material showed high efficiency in mineralizing ^{14}C-ring-labeled IPU, similar to the mineralization rates recorded for the soil that was used for the preparation of the biobed packing material (33). The enhanced IPU mineralization capacity recorded for the biobed packing material may also result from its frequent exposure to IPU-containing effluents (four times in 2015) (see Table S1 in the supplemental material). This is in accordance with the results of Sniegowski et al., who showed that the addition of small amounts of soil adapted to the enhanced biodegradation of linuron (another phenylurea herbicide), metamitron, and metalaxyl resulted in the rapid establishment of a high mineralization potential for these pesticides in biobeds, whereas nonprimed biobeds also developed a linuron mineralization capacity but only after repeated applications of linuron (34, 35). Mass balance analysis of the applied ^{14}C-labeled IPU suggested that all the extractable (and, hence, bioavailable) ^{14}C-labeled IPU evolved to $^{14}CO_2$. The proportion of NER in the biobed packing material (37%) was similar to that in the soils of the INRAE farm (40 to 50%) (24) but lower than those observed in soils not adapted to the enhanced biodegradation of IPU (48 to 73%) (36).

The rapid mineralization of ^{14}C-labeled IPU accompanied by a reciprocal increase in the abundance of the *pdmA* gene suggests that the IPU-degrading microbial guild, carrying the *pdmA* gene, was already present in the biobed packing material and readily proliferated upon a fresh IPU addition. Measurements of the transcription pattern of the *pdmA* gene in the biobed packing material confirmed the direct involvement of the IPU-degrading guild in the rapid mineralization of this herbicide. This is in line with previous studies reporting a positive correlation between the mineralization of linuron and the abundance of the *libA* or *hylA* gene, involved in the hydrolysis of linuron, in biobed packing material (12). Interestingly, when no more bioavailable IPU remained, the abundance and transcription levels of *pdmA* had reverted to their initial levels. This is in agreement with studies showing that the 2,4-dichlorophenoxyacetic acid (2,4-D)-,

4-chloro-2-methylphenoxyacetic acid (MCPA) (37)-, and atrazine (38)-degrading genetic potential rapidly decreased once pesticide mineralization had ceased in soils.

All these findings suggest that IPU application to the biobed packing material stimulated the proliferation of the IPU-degrading bacterial guild. Beyond this, we explored the overall effect of IPU on the total bacterial community and its active fraction. The bacterial community of the biobed packing material was dominated by *Proteobacteria*, in line with recent studies of biobed systems (9, 10). The total and active fractions of the genera *Sphingomonas* and *Sphingobium* were not changed in response to IPU exposure, suggesting that the *pdmAB*-carrying sphingomonads constitute only a small fraction of the sphingomonads and/or that the *pdmAB* genes are also carried by bacteria other than sphingomonads. When applied at an agronomic dose, IPU did not induce significant effects on the α- and β-diversities of the bacterial community of the biobed packing material. This is in line with a study by Storck et al., who reported no effects of IPU on the soil bacterial community even when exposed at 10 times the agronomical dose (20). In addition, no changes in the active fraction of the bacterial community in the biobed packing material were observed in response to IPU, suggesting that the transitory changes of the IPU-degrading bacterial guild can be traced only at the functional level (*pdmA* gene) but not at the overall bacterial community level, even with advanced sequencing approaches. This shortcoming might be overcome with stable isotope probing with ^{13}C-labeled IPU, which would narrow down the analysis to the IPU-degrading guild (39).

We noticed that *pdmA* sequences were more abundant than pSH, suggesting that pSH was not the only genetic element harboring *pdmA* in the biobed packing material. To shed light on the genomic location of the *pdmAB* genes, their localization in the metagenome of the bacterial community was studied. Sequencing of four fosmids carrying the *pdmA* gene showed that the *pdmAB* genes resided in a cassette with an organization identical to those of *Sphingomonas* sp. SH and *Sphingobium* sp. YBL2. The sole exception was fosmid 14, carrying an incomplete *pdmAB* cassette, implying that it was still under evolution.

The high level of conservation of the *pdmAB* cassette and its flanking by MGEs suggest the involvement of horizontal gene transfer mechanisms in its dispersal among IPU-degrading bacteria. MGEs in the *pdmAB* region belonged to the Tn*3*, IS*6*, and IS*256* families. Tn*3* transposases, forming composite transposons carrying catabolic operons (40), were mostly remnants of previous insertions, suggesting a limited role in the recent transposition of *pdmAB*. IS*6* family ISs, composed of a transposase gene (789 to 880 bp) flanked by short TIRs (10 to 20 bp) and DRs (8 bp) (41), were the most common MGEs in the *pdmAB* region. Members of this IS family, like IS*6100*, are often associated with the transposition of catabolic operons such as *lin* in a hexachlorocyclohexane-degrading *Sphingomonas* sp. (42) and *car* in carbazole-degrading *Sphingomonas* sp. strain XLDN2-5 (43). Several copies of IS*6* (fosmids 14 and 16 and YBL2-p4) were truncated, lacking their binding domain at the N terminus, which is most probably the result of a lateral insertion of an IS*256* element. This was reinforced by the detection of intact TIRs and DRs in all IS*256* copies, unlike IS*6* elements, which often lacked TIRs and DRs in their flanking regions. Intact IS*256* elements were also found downstream of the *pdmAB* operon in fosmids 13 and 15. IS*256* family MGEs form composite transposons (44, 45) enabling the dispersal of catabolic operons such as the tetrachloroethene reductive dehalogenase operon of *Desulfitobacterium hafniense* (46). The presence of several remnants of Tn*3* and identical IS*6* elements in the *pdmAB* genomic region suggests their ancestral role in the transposition of the *pdmAB* operon and their gradual degeneration by lateral insertion events. The role of IS*6* in *pdmAB* operon transposition is further supported by the organization of the MGEs in pSH, where both sides of the *pdmAB* operon are flanked by IS*6* family transposases (named *tnpX* in its first report by Gu et al. [22]), forming a composite transposon (not interrupted by IS*256*). The probable lateral insertion of IS*256* observed in our fosmids and YBL2-p4 could be associated with a potential halting of the further dispersal of the catabolic operon since truncated transposases have been shown to inhibit transposition (41). Alternatively, the insertion

of IS*256* might introduce a promoter −35 hexamer enhancing the transcription of the catabolic operon, as previously observed in *Paracoccus* spp. (47). However, a search of the relevant insertion regions failed to identify promoter motifs. Overall, our analysis suggests that the *pdmAB* region is a battlefield of insertion events, with IS*6* being crucial in the initial evolution and dispersal of *pdmAB*. This capacity is most probably relayed to IS*256*, whose exact role in the transposition or activation of the *pdmAB* operon warrants further study.

We observed limited synteny between the fosmids and pSH, verifying our initial hypothesis that the *pdmAB* cassette may reside in genetic structures other than pSH. Hence, we further aimed to discern the origin of the fosmid replicons containing *pdmAB*. Fosmids 13, 15, and 16 were rich in genes encoding conjugation transfer proteins (*traACDG* and *mobA*) and plasmid partitioning genes (*parAB*), suggesting that they originate from conjugative plasmids (44, 45, 48–50). They constituted mosaics of plasmid-borne genes previously found in sphingomonads involved in the catabolism of IPU (*Sphingobium* sp. YBL2 and *Sphingomonas* sp. SH) or chloramphenicol (*Sphingobium* sp. strain CAP-1) (D. G. Karpouzas and S. Vasileiadis, unpublished data). Our results are in line with those of a comparative genomic analysis of different IPU-degrading sphingomonad strains by Yan et al. (23) and strongly suggest that the *pdmAB* cassette is a common component of catabolic plasmids in IPU-degrading sphingomonads (51). These results provide further confirmation of the key role of sphingomonads in the degradation of organic pollutants (52), which stems from their remarkable capacity to recruit catabolic genes and evolve novel catabolic pathways through horizontal gene transfer (23, 53, 54).

Fosmid 14 showed limited synteny with pSH and YBL2-p4, lacked any gene signatures of plasmid origin, and contained genes participating in housekeeping biosynthetic processes in bacteria. This suggests that the content of fosmid 14 was of a chromosomal origin belonging to the family *Xanthomonadaceae* and especially to the genus *Rhodanobacter*. Bacteria of this genus are known as denitrifiers (55) and organic pollutant degraders in terrestrial ecosystems (56). A recent metagenomic analysis in a metal-contaminated groundwater aquifer identified *Rhodanobacter* bacteria as dominant members of the bacterial community (57). This was attributed to the presence in their pangenome of recombinational hot spots that allow the lateral gene transfer of metal resistance genes. These findings suggest that the *pdmAB* cassette was recently acquired and integrated into the genome of a *Rhodanobacter* sp. The detection of *pdmAB* in a chromosomal fragment of a *Rhodanobacter* species is challenging our knowledge that these genes exhibit a peculiar specificity for members of the *Sphingomonas* genus. Further studies will explore the extent of *pdmAB* dispersal to nonsphingomonad bacteria.

To conclude, IPU application to biobed packing material triggered the proliferation and transcription activity of *pdmA* but did not induce any detectable distinct alterations in the compositions of the total and active bacterial communities. Metagenomic analysis provided novel insights into the evolution, localization, and dispersal mechanisms of the *pdmAB* genes. These reside in a highly conserved cassette, flanked by IS*6* and IS*256* MGEs that drive the transposition and/or activation of *pdmAB*, and are localized in distinct sphingomonad plasmids. However, their integration into the genome of *Gammaproteobacteria* prone to recombination also occurs. These findings underline the high mobility of the *pdmAB* cassette and reinforce the function of on-farm biobed systems as hot spots for the evolution of novel pesticide catabolic traits, thereby used as genetic pools for further biotechnological exploitation.

MATERIALS AND METHODS

Biobed packing material characteristics and sampling. The biobed packing material was collected from the biobed of the experimental farm of INRAE, Dijon, France (Bretenière [47°14′25.6″N, 5°06′12.4″E {Google Maps}]), in June 2015. It was prepared by mixing straw with a mixture of soils (36.7% clay, 43.6% silt, and 19.7% sand) collected from different fields of the experimental farm, among which was soil exhibiting a high IPU mineralization capacity (24). The biobed packing material had an organic matter content of 10.2% and a pH of 7.0. The biobed had received pesticides contained in rinsates, washates,

and spraying remnants in 2015, as listed in Table S1 in the supplemental material. Upon its collection, the biobed packing material was sieved through a 5-mm-mesh sieve and stored at 4°C until use.

Experimental setup of three microcosm studies. For microcosm experiment 1 (Fig. 1), the biobed packing material was initially moistened to 80% of its water-holding capacity (WHC) (70.19%), and this moisture level was maintained throughout the incubation period. It was then treated with the recommended agronomical dose of 2 mg IPU (99% purity; Riedel-de-Haen) (applied in a methanolic solution) per kg (dry weight) of packing material. A first triplicate set of 20-g samples was removed and further treated with 1.7 kBq of ^{14}C-ring-labeled IPU (99% radiochemical purity; specific activity of 666,000 kBq mmol^{-1}) (International Isotopes, Munich, Germany) to assess IPU mineralization. Immediately after the application of ^{14}C-ring-labeled IPU (0 days) and 2, 4, 7, and 14 days later, the mineralization of ^{14}C-ring-labeled IPU to $^{14}CO_2$ was analyzed as described below. In parallel, a second triplicate set of 20-g samples (not further treated with ^{14}C-ring-labeled IPU) was prepared to determine the abundances of *pdmA* and pSH parallel to IPU mineralization. Subsamples (250 mg) of these microcosms were collected at days 0, 4, 7, and 14 and stored at −20°C before being used for DNA extraction and qPCR as described below. For both series, all microcosms were incubated at 20°C in the dark.

For microcosm experiment 2, the biobed packing material was moistened to 50% of its water-holding capacity, which was maintained throughout the incubation period. A sample of the biobed packing material was separated into 20-g microcosms that were pretreated with either 2 mg IPU (aqueous solution) per kg (dry weight) of packing material or the same amount of water without IPU to serve as an untreated control. The microcosms were incubated at 20°C in the dark for 35 days. Upon the completion of this pretreatment period, the IPU-treated or nontreated microcosms were retreated with IPU (2 mg/kg [dry weight]) or received the same amount of water without IPU, respectively. To determine IPU mineralization, immediately after the second IPU exposure, triplicate microcosms of 5 g were treated with 1.3 kBq of ^{14}C-ring-labeled IPU. Immediately after the application of ^{14}C-ring-labeled IPU (0 days) and 2, 4, 7, 10, 14, 16, and 18 days after treatment, IPU mineralization was determined as described below. To assess the abundance and expression of the *pdmA* gene parallel to IPU mineralization, 2 g of biobed packing material was sampled from both the treated and control microcosms at days 0, 4, 7, 10, and 18 and stored at −80°C until DNA/RNA extraction and downstream qPCR and reverse transcription-qPCR (RT-qPCR) as described below. Finally, the potential impact of IPU on the diversity of the bacterial community of the biobed packing material was determined at days 0, 7, 10, and 18 by DNA- and RNA-based Illumina 16S amplicon sequencing as described below.

For microcosm experiment 3, 200 g of biobed packing material was moistened to 50% of its water-holding capacity (which was kept constant during the experiment) and subjected to three repeated IPU applications (5 mg/kg [dry weight]) within 100 days. At the end of the treatment period, triplicate 5-g samples were removed and used for high-molecular-weight DNA extraction and subsequent construction of metagenomic fosmid libraries as described below.

Mineralization of ^{14}C-ring-labeled IPU in the biobed packing material. In microcosm experiments 1 and 2, IPU mineralization of ^{14}C-ring-labeled IPU was measured by the evolution of $^{14}CO_2$ trapped in 5 ml of 0.2 M sodium hydroxide. This was mixed with 10 ml scintillation liquid (ACII scintillation fluid; Amersham) and analyzed by liquid scintillation counting (LS 6500 multipurpose scintillation counter; Beckman Coulter, Brea, CA, USA). IPU mineralization parameters were determined as described previously (33).

At the end of the incubation period of microcosm experiment 2, ^{14}C mass balance analysis was performed by measuring the amounts of radioactive ERs and NERs in the biobed packing material. To determine the ER fraction, 10 ml of methanol was added to each sample, which was then thoroughly mixed and placed on a rotary shaker at 150 rpm for 24 h. After centrifugation for 10 min at 6,000 × *g*, the supernatant was recovered, and 5-ml aliquots were mixed with scintillation liquid and measured for radioactivity by liquid scintillation counting. The remaining biobed packing material was recovered and entirely dried at ambient temperature. The ^{14}C-labeled NERs were determined by the combustion of 0.5 g of dried packing material under O_2 flow at 900°C for 4 min using an OX-500 biological oxidizer (EG&G Instruments, France), as previously described (58). The mass balance of ^{14}C-labeled residues was calculated as a percentage of the total amount of ^{14}C radioactivity retrieved from the different fractions (i.e., $^{14}CO_2$-labeled residues and ^{14}C-labeled ERs and NERs).

DNA and RNA extraction from the biobed packing material. In microcosm experiment 1, DNA was extracted from 250-mg soil samples according to the ISO 11063 method (59), initially described by Martin-Laurent et al. (60). DNA concentrations were determined with a Thermo Fisher StepOne Plus thermocycler (Applied Biosystems) by using fluorescent dye from a Quant-iT PicoGreen dsRNA assay kit (Invitrogen).

In microcosm experiment 2, RNA and DNA were coextracted from 2-g soil samples with the PowerSoil RNA isolation kit and a DNA coelution accessory kit (Mobio, Carlsbad, CA, USA), respectively. A DNase treatment step (DNase Max kit; Mobio, Carlsbad, CA) was performed to obtain DNA-free RNA extracts. The possibility of DNA contamination was further excluded by checking for the absence of 16S rRNA gene amplicons by PCR. The extracted RNA and DNA were quantified with a Nanodrop ND1000 spectrophotometer (NanoDrop Technologies Inc.).

In microcosm experiment 3, high-molecular-weight DNA was extracted using the protocol described previously by Zhou et al. (61).

qPCR analysis of the abundance of the 16S rRNA gene, the *pdmA* gene, and the pSH region. In microcosm experiment 1, prior to the quantification of target sequences, the absence of PCR inhibitors in the DNA extracts was verified as previously described (62). The abundance of total bacteria was measured by qPCR, according to the ISO 17601 method (63), targeting the 16S rRNA gene with the

TABLE 1 Primers used in the present study

Primer pair	Gene target	Purpose(s)	Sequence (5′–3′)	Reference
U341_F	16S rRNA	Amplicon sequencing	CCTACGGGNBGCASCAG	20
U805_R			GACTACNVGGGTATCTAATCC	
pdmA_F	*pdmA*	qPCR, RT-qPCR, and PCR detection in fosmid libraries	TGGCAGTTCAGCTATGATGC	This study
pdmA_R			ATAGTCCCCTTTGCCTTCGT	
pSH_F	pSH region	qPCR	GGCTTGGGTACGCTATGAAA	This study
pSH_R			CGTTCAGGACTGCCGTAAAG	
341_F	16S rRNA	qPCR and RT-qPCR	CCTACGGGAGGCAGCAG	64
534_R			ATTACCGCGGCTGCTGGCA	

universal bacterial primer pair 341_F-534_R as described previously (64). The abundance of bacteria carrying the *pdmA* gene was determined by qPCR using primer pair pdmA_F-pdmA_R (228 bp), designed based on the sequence of the *pdmA* gene reported previously by Gu et al. (22). The abundance of the *pdmAB*-carrying plasmid pSH was determined by qPCR with primer pair pSH_F-pSH_R. These primers were designed to amplify a region on pSH of the IPU-degrading *Sphingomonas* sp. strain SH (bp 8596 to 8792 on pSH) (Fig. S2) (24). The selection of this specific region to quantify pSH by qPCR instead of a region picked in the backbone of the plasmid (i.e., *rep*, *kor*, or *trfA*) ensured high specificity and minimal nontarget amplification. The sequences of all primers used in the present study are given in Table 1. All qPCRs were performed in a 15-μl volume that was composed of SYBR green PCR master mix (Absolute qPCR SYBR green Rox; ABgene), 100 ng of T4 gp32 (Qbiogene), 2 μM relevant primers, and 0.4 ng of template DNA. The qPCR conditions were 95°C for 15 min, followed by 35 cycles of 95°C for 15 s, 60°C for 30 s, and 72°C for 30 s. Data acquisition was performed at 80°C. After amplification, melting curves were obtained by increasing the temperature from 80°C to 95°C (+0.5°C/s). Calibration curves were established from previously cloned *pdmA* and pSH region PCR products of the IPU-degrading *Sphingomonas* sp. strain SH (24). Nontemplate controls (NTCs) were included in all qPCR assays.

RT-qPCR analysis of transcription of the 16S rRNA and *pdmA* genes. In microcosm experiment 2, the numbers of transcripts of the 16S rRNA and *pdmA* genes in the biobed packing material were determined by RT-qPCR performed with the Go*Taq* one-step RT-qPCR system (Promega, Madison, WI, USA). Reaction mixtures contained 7.5 μl of 2× Go*Taq* qPCR master mix, 0.3 μl of 50× GoScript RT mix, 0.25 μl of carboxy-X-rhodamine reference dye (30 μM; Promega, Madison, WI, USA), 1 μM each primer (Eurogentec, Liège, Belgium), 0.1 ng (for 16S rRNA) or 2 ng (for *pdmA*) of RNA, and ultrapure sterile water to a total volume of 15 μl. Thermal conditions were 15 min at 40°C and 10 min at 95°C, followed by 40 cycles of 95°C for 15 s, 60°C for 30 s, and 72°C for 30 s; data acquisition at 80°C for 15 s; and a melting-curve stage for 15 s at 95°C, 1 min at 72°C, and 15 s at 95°C. Four independent replicates for each treatment and three NTCs were used for each RT-qPCR assay. Calibration curves were obtained as described above for microcosm study 1.

Amplicon sequencing of the total (DNA) and active (RNA) bacterial communities. In microcosm experiment 2, the diversity of total and active bacteria in the biobed packing material was assessed by deep sequencing of 16S rRNA amplicons obtained from DNA and RNA (cDNA) templates. Total cDNA was obtained from DNA-free RNA using the Go*Taq* reverse transcription system (Promega, Madison, WI, USA) with random hexamers according to the manufacturer's instructions. Reverse transcription efficiency was checked by qPCR under the same conditions as the ones described above. For both DNA and cDNA, a two-step amplification approach targeting the V3-V4 ultravariable region of the 16S rRNA gene sequence was used. First-step PCR was performed using the universal bacterial primers U341_F and 805_R (Table 1) with overhang adapters (forward adapter TCGTCGGCAGCGTCAGATGTGTATAAGAGACAG and reverse adapter GTCTCGTGGGCTCGGAGATGTGTATAAGAGACAG). The resulting amplicons were used as the templates in a second PCR carried out with multiplexed primers containing the universal overhang adapters and specific barcodes. The first-step PCR mix contained 2 ng of DNA or cDNA as the template, 7.5 μl of 2× Phusion high-fidelity PCR master mix (Thermo Scientific, Waltham, MA, USA), 250 ng of T4 gene 32 protein (MP Biomedicals, Santa Ana, CA, USA), 0.375 μl of each primer (10 μM), and ultrapure sterile water to a total volume of 15 μl. Thermal conditions were 3 min at 98°C and 25 cycles at 98°C for 30 s, 55°C for 30 s, and 72°C for 30 s, followed by a final extension step for 10 min at 72°C. Duplicates from each PCR were pooled, and a 6-μl aliquot was then used as the template to carry out eight further amplification cycles with the barcoded primers containing the adapters. Second-step PCR was performed using a 384 Nextera XT index kit (Illumina, San Diego, CA, USA) for the addition of multiplexing index sequences. It was carried out in 30-μl reaction volumes containing 2.5 μl of sterile water, 15 μl of 2× Phusion HF master mix (Thermo Scientific, Waltham, MA, USA), 250 ng of T4 gp32 (MP Biomedicals, Santa Ana, CA, USA), 3 μl of each primer (10 μM), and 6 μl of the StepOne PCR product (Applied Biosystems). Thermal cycling conditions were 98°C for 3 min, followed by eight cycles of 98°C for 30 s, 55°C for 30 s, and 72°C for 30 s, with a final extension step at 72°C for 10 min. The size of the amplicons was verified by electrophoresis on a 2% agarose gel. PCR products were purified (amplicon library purification, PicoGreen quantification, and pooling) and sequenced (Illumina MiSeq 2 by 300 bp) by Microsynth (Balgach, Switzerland).

Metagenomic analysis of the biobed packing material. In microcosm experiment 3, purified high-molecular-weight DNA was cloned in the fosmid vector pCC1FOS (Epicentre, Chicago, IL, USA) and then transferred to *Escherichia coli* EPI300-T1R according to the manufacturer's protocol. Transformed cells were spread on LB agar plates containing chloramphenicol (15 mg/liter) and arabinose (0.01%) and incubated for 16 h at 37°C. Approximately 10,000 colonies were picked and inoculated into 96-well plates containing 200 μl of liquid LB medium amended with chloramphenicol (15 mg/liter) and arabinose (0.01%) (in total, 105 96-well plates were prepared). All plates were incubated overnight at 37°C and then replica transferred onto LB agar plates containing chloramphenicol and arabinose. The 96 growing colonies per plate were pooled with 2 ml of sterilized ultrapure water, and the bacterial pellet was used for fosmid DNA extraction using the Isolate II plasmid minikit (Bioline, Memphis, TN, USA). The pooled fosmid DNA extracted from each plate was subjected to PCR with primer pair pdmA_F-pdmA_R (Table 1). PCR mixtures (30 μl) included 1× polymerase buffer containing $MgCl_2$, 0.2 mM deoxynucleoside triphosphates (dNTPs), 0.4 μM each primer, 2 ng of DNA, 1 U of Kapa*Taq* DNA polymerase (Kapa Biosystems, Wilmington, MA, USA), and sterile ultrapure water up to the reaction volume of 30 μl. Thermal cycling PCR conditions were 95°C for 1 min, followed by 38 cycles (for *pdmA* amplification) of 30 s at 95°C, 30 s at 60°C, and 40 s at 72°C, with a final extension step for 5 min at 72°C. Fosmid pools positive for *pdmA* were identified via agarose gel electrophoresis (1.5%). Glycerol stocks of the *pdmA*-positive plates were grown in fresh 96-well plates, replica plated on LB plates, and then tested by colony PCR for the presence of the *pdmA* gene. Fosmids positive for the presence of *pdmA* were sequenced at the Brigham Young University (Provo, UT, USA) DNA Sequencing Center with the Illumina HiSeq system in rapid mode for the generation of 250-bp paired-end and mate pair reads for each sample.

Data analysis. (i) Statistical analysis of qPCR and RT-qPCR data. In microcosm experiments 1 and 2, statistical analysis of variance (ANOVA) was done using XLstat. The normality of the data was checked (Shapiro-Wilk test with a P value of >0.05), and the homogeneity of variances was verified (Levene's test with a P value of >0.05) for each treatment and time point. For parametric distributions, data were compared using ANOVA followed by Tukey's test and Student's t test (P value of 0.05 [significant] or 0.01 [very significant]). For nonparametric distributions, data were compared using a Kruskal-Wallis test followed by a Conover-Iman test with Bonferroni-corrected P values and a Welch test (P value of 0.05) for pairwise comparisons.

(ii) Bioinformatic and statistical analyses of amplicon sequencing data. In microcosm experiment 2, amplicon sequencing data were analyzed using an in-house-developed Python pipeline together with different bioinformatic tools (available upon request). 16S rRNA gene sequences were assembled using PEAR software (65) with default settings. Further quality checks were conducted using the QIIME 1 pipeline (66). Sequences of <348 bp were removed. Reference-based and *de novo* chimera detection as well as clustering into OTUs were performed with VSEARCH software (67) using appropriate reference databases (Greengenes' representative set of 16S rRNA gene sequences) with a threshold placed at 93% identity. Representative sequences for each OTU were aligned using PyNAST (68). Phylogenetic trees were constructed using FastTree (69). Taxonomy was assigned using UCLUST (70) and the latest-release Greengenes database (v.05/2013) for 16S rRNA gene sequences (71). Bacterial α-diversity indices pertaining to richness (Chao1), evenness (Simpson reciprocal), and relatedness (phylogenetic diversity whole tree) were calculated based on rarefied OTU tables (64,000 sequences used per sample). UniFrac distance matrices (72) were also computed to detect global variations in the composition of bacterial communities. Differences in phylum composition were determined using a comparative bar chart. Phyla with relative abundances of $<0.05\%$ were excluded from this analysis. Principal-coordinate analysis (PCoA) of OTU-weighted UniFrac distance matrices was performed and plotted with QIIME. Analysis of similarity (ANOSIM) was performed with QIIME to identify significant differences (P value of <0.05 or 0.01) at the community level between treatments. Subsequent pairwise analyses were performed using Primer 7 statistical software (P value of 0.05) (PrimerE, Ivy Bridge, United Kingdom).

(iii) Bioinformatic analysis of fosmids obtained from metagenomic libraries. In microcosm experiment 3, the output sequencing data were screened with FastQC v0.11.8 (73) and quality trimmed with Trimmomatic v0.22 (74) using default parameters and library prep kit-associated adapter removal. Properly paired sequences were further checked for adapter remains in the case of the mate pair libraries with NxTrim v0.4.3-778bea9 software (75). Good-quality and properly oriented trimmed sequences, of 50× minimum coverage for the paired-end and mate pair data sets (100× combined), were used for assembling the fosmid sequences with Allpaths-LG v52488 (76). The pCC1FOS fosmid vector (GenBank accession number EU140751.1) was manually removed from the resulting contigs with Unipro UGENE v1.31 (77), and scaffolding was performed with SSPACE v2.0 (78) using default parameters. Sequence structural and functional annotation was performed with Prokka v1.12 (79) with default parameters/tools/databases and was manually curated according to the more up-to-date National Center for Biotechnology Information (NCBI) International Nucleotide Sequence Database Collaboration (INSDC) nonredundant (nr) nucleotide database (80), using Basic Local Alignment Search Tool (BLAST) v2.7.1+ (81). The sequences of the predicted ORFs were compared between the different fosmid inserts (GenBank accession numbers MK304431 for fosmid 13, MK304432 for fosmid 14, MK304433 for fosmid 15, and MK304434 for fosmid 16) and the plasmids pSH (GenBank accession number KU237244.1) and YBL2-p4 (GenBank accession number KC904972) with BLAST, and synteny plots were produced with the genoPlotR v0.8.7 package (82) in R v3.3.3 (83). Fosmid insert taxonomies were inferred according to the lowest common ancestor (LCA) algorithm for a minimum of 5 consensus BLAST hits against the NCBI nr database with metagenome analyzer (MEGAN 6 community edition) v6.1.37beta software (84). Further analysis was performed to identify MGEs such as ISs, transposases, and their TIRs and DRs on the fosmids,

pSH, and YBL2-p4 using ISEscan v1.7.1 (85), ISsaga (86) for ISfinder database v14-Mar-2019 (87), and the OASIS software implementation (88) of the ISsaga application.

Data availability. Sequences were deposited in the GenBank Sequence Read Archive (SRA) database under accession number PRJNA494388.

SUPPLEMENTAL MATERIAL

Supplemental material is available online only.

SUPPLEMENTAL FILE 1, PDF file, 1.3 MB.

SUPPLEMENTAL FILE 2, XLSX file, 0.02 MB.

ACKNOWLEDGMENTS

The Ph.D. studies of V. Storck performed at the Doctoral School of Environment and Health (ED E2S) at the University of Burgundy (grant number 2013-31) were funded by the French Ministry of Education and Research (MESR). Parts of this study (S. Gallego) were performed within the frame of the IAPP-MCSA-FP7 project Love-To-Hate. C. Perruchon was supported by the project Synthetic Biology: from Omics Technologies to Genomic Engineering (OMIC-ENGINE) (MIS 5002636), which is implemented under the action Reinforcement of the Research and Innovation Infrastructure, funded by the operational program Competitiveness, Entrepreneurship, and Innovation (NSRF 2014-2020) and cofinanced by Greece and the European Union (European Regional Development Fund). S. Vasileiadis was supported by MSCA-IF-H2020 EMIGRATE.

REFERENCES

1. Lewis SL, Maslin MA. 2015. Defining the Anthropocene. Nature 519:171–180. https://doi.org/10.1038/nature14258.
2. De Wilde T, Spanoghe P, Debaer C, Ryckeboer J, Springael D, Jaeken P. 2007. Overview of on-farm bioremediation systems to reduce the occurrence of point source contamination. Pest Manag Sci 63:111–128. https://doi.org/10.1002/ps.1323.
3. Masiá A, Campo J, Vázquez-Roig P, Blasco C, Picó Y. 2013. Screening of currently used pesticides in water, sediments and biota of the Guadalquivir River Basin (Spain). J Hazard Mater 263:95–104. https://doi.org/10.1016/j.jhazmat.2013.09.035.
4. Torstensson L, Castillo MDP. 1996. Biobeds minimise environmental risks when filling agricultural spraying equipment, p 223–224. *In* Pesticides in soil and the environment. Proceedings of the COST 66 Workshop, Stratford-upon-Avon, United Kingdom, 13 to 15 May 1996.
5. Pussemier L, De Vleeschouwe C, Debongnie P. 2004. Self-made biofilters for onfarm clean-up of pesticides wastes. Outlooks Pest Manag 15:60–63. https://doi.org/10.1564/15apl06.
6. Vischetti C, Capri E, Trevisan M, Casucci C, Perucci P. 2004. Biomassbed: a biological system to reduce pesticide point contamination at farm level. Chemosphere 55:823–828. https://doi.org/10.1016/j.chemosphere.2003.11.042.
7. Karas PA, Perruchon C, Karanasios E, Papadopoulou ES, Manthou E, Sitra S, Ehaliotis C, Karpouzas DG. 2016. Integrated biodepuration of pesticide-contaminated wastewaters from the fruit-packaging industry using biobeds: bioaugmentation, risk assessment and optimized management. J Hazard Mater 320:635–644. https://doi.org/10.1016/j.jhazmat.2016.07.071.
8. Castillo MDP, Torstensson L, Stenstrom J. 2008. Biobeds for environmental protection from pesticide use—a review. J Agric Food Chem 56:6206–6219. https://doi.org/10.1021/jf800844x.
9. Bergsveinson J, Perry BJ, Sheedy C, Braul L, Reedyk S, Gossen BD, Yost CK. 2018. Identifying the core bacterial and fungal communities within four agricultural biobeds used for the treatment of pesticide rinsates. J Appl Microbiol 125:1333–1342. https://doi.org/10.1111/jam.14051.
10. Holmsgaard PN, Dealtry S, Dunon V, Heuer H, Hansen LH, Springael D, Smalla K, Riber L, Sorensen SJ. 2017. Response of the bacterial community in an on-farm biopurification system, to which diverse pesticides are introduced over an agricultural season. Environ Pollut 229:854–862. https://doi.org/10.1016/j.envpol.2017.07.026.
11. Dunon V, Bers K, Lavigne R, Top EM, Springael D. 2018. Targeted metagenomics demonstrates the ecological role of IS1071 in bacterial community adaptation to pesticide degradation. Environ Microbiol 20:4091–4111. https://doi.org/10.1111/1462-2920.14404.
12. Horemans B, Bers K, Romero ER, Juan EP, Dunon V, De Mot R, Springael D. 2016. Functional redundancy of linuron degradation in microbial communities in agricultural soil and biopurification systems. Appl Environ Microbiol 82:2843–2853. https://doi.org/10.1128/AEM.04018-15.
13. Bælum J, Prestat E, David MM, Strobel BW, Jacobsen CS. 2012. Modeling of phenoxy acid herbicide mineralization and growth of microbial degraders in 15 soils monitored by quantitative real-time PCR of the functional tfdA gene. Appl Environ Microbiol 78:5305–5312. https://doi.org/10.1128/AEM.00990-12.
14. Monard C, Martin-Laurent F, Lima O, Devers-Lamrani M, Binet F. 2013. Estimating the biodegradation of pesticide in soils by monitoring pesticide-degrading gene expression. Biodegradation 24:203–213. https://doi.org/10.1007/s10532-012-9574-5.
15. Piutti S, Hallet S, Rousseaux S, Philippot L, Soulas G, Martin-Laurent F. 2002. Accelerated mineralisation of atrazine in maize rhizosphere soil. Biol Fertil Soils 36:434–441. https://doi.org/10.1007/s00374-002-0545-6.
16. Rousidou C, Karaiskos D, Myti D, Karanasios E, Karas PA, Tourna M, Tzortzakakis EA, Karpouzas DG. 2017. Distribution and function of carbamate hydrolase genes cehA and mcd in soils: the distinct role of soil pH. FEMS Microbiol Ecol 93:fiw219. https://doi.org/10.1093/femsec/fiw219.
17. Itoh H, Navarro R, Takeshita K, Tago K, Hayatsu M, Hori T, Kikuchi Y. 2014. Bacterial population succession and adaptation affected by insecticide application and soil spraying history. Front Microbiol 5:457. https://doi.org/10.3389/fmicb.2014.00457.
18. Gallego S, Devers-Lamrani M, Rousidou K, Karpouzas DG, Martin-Laurent F. 2019. Assessment of the effects of oxamyl on the bacterial community of an agricultural soil exhibiting enhanced biodegradation. Sci Total Environ 651:1189–1198. https://doi.org/10.1016/j.scitotenv.2018.09.255.
19. Karpouzas DG, Kandeler E, Bru D, Friedel I, Auer Y, Kramer S, Vasileiadis S, Petric I, Udikovic-Kolic N, Djuric S, Martin-Laurent F. 2014. A tiered assessment approach based on standardized methods to estimate the impact of nicosulfuron on the abundance and function of the soil microbial community. Soil Biol Biochem 75:282–291. https://doi.org/10.1016/j.soilbio.2014.04.022.
20. Storck V, Nikolaki S, Perruchon C, Chabanis C, Sacchi A, Pertile G, Baguelin C, Karas PA, Spor A, Devers-Lamrani M, Papadopoulou ES, Sibourg O, Malandain C, Trevisan M, Ferrari F, Karpouzas DG, Tsiamis G, Martin-Laurent F. 2018. Lab to field assessment of the ecotoxicological impact of chlorpyrifos, isoproturon, or tebuconazole on the diversity and composition of the soil bacterial community. Front Microbiol 9:1412. https://doi.org/10.3389/fmicb.2018.01412.
21. Vasileiadis S, Puglisi E, Papadopoulou ES, Pertile G, Suciu N, Pappolla RA, Tourna M, Karas PA, Papadimitriou F, Kasiotakis A, Ipsilanti N, Ferrarini A, Sułowicz S, Fornasier F, Menkissoglu-Spiroudi U, Nicol GW, Trevisan M, Karpouzas DG. 2018. Blame it on the metabolite: 3,5-dichloroaniline rather than the parent compound is responsible for the decreasing

diversity and function of soil microorganisms. Appl Environ Microbiol 84:e01536-18. https://doi.org/10.1128/AEM.01536-18.
22. Gu T, Zhou CY, Sorensen SR, Zhang J, He J, Yu PW, Yan X, Li SP. 2013. The novel bacterial N-demethylase PdmAB is responsible for the initial step of N,N-dimethyl-substituted phenylurea herbicide degradation. Appl Environ Microbiol 79:7846–7856. https://doi.org/10.1128/AEM.02478-13.
23. Yan X, Gu T, Yi ZQ, Huang JW, Liu XW, Zhang J, Xu XH, Xin ZH, Hong Q, He J, Spain JC, Li SP, Jiang JD. 2016. Comparative genomic analysis of isoproturon-mineralizing sphingomonads reveals the isoproturon catabolic mechanism. Environ Microbiol 18:4888–4906. https://doi.org/10.1111/1462-2920.13413.
24. Hussain S, Devers-Lamrani M, El Azhari N, Martin-Laurent F. 2011. Isolation and characterization of an isoproturon mineralizing Sphingomonas sp. strain SH from a French agricultural soil. Biodegradation 22:637–650. https://doi.org/10.1007/s10532-010-9437-x.
25. Nielsen TK, Sorensen SR, Hansen LH. 2015. Draft genome sequence of isoproturon-mineralizing Sphingomonas sp. SRS2, isolated from an agricultural field in the United Kingdom. Genome Announc 3:e00569-15. https://doi.org/10.1128/genomeA.00569-15.
26. Dealtry S, Holmsgaard PN, Dunon V, Jechalke S, Ding GC, Krogerrecklenfort E, Heuer H, Hansen LH, Springael D, Zuhlke S, Sorensen SJ, Smalla K. 2014. Shifts in abundance and diversity of mobile genetic elements after the introduction of diverse pesticides into an on-farm biopurification system over the course of a year. Appl Environ Microbiol 80:4012–4020. https://doi.org/10.1128/AEM.04016-13.
27. Dunon V, Sniegowski K, Bers K, Lavigne R, Smalla K, Springael D. 2013. High prevalence of IncP-1 plasmids and IS1071 insertion sequences in on-farm biopurification systems and other pesticide-polluted environments. FEMS Microbiol Ecol 86:415–431. https://doi.org/10.1111/1574-6941.12173.
28. Chaudhuri S, Anton IA, Coggins JR. 1987. Shikimate dehydrogenase from Escherichia coli. Methods Enzymol 142:315–320. https://doi.org/10.1016/s0076-6879(87)42042-9.
29. Lobley CMC, Aller P, Douangamath A, Reddivari Y, Bumann M, Bird LE, Nettleship JE, Brandao-Neto J, Owens RJ, O'Toole PW, Walsh MA. 2012. Structure of ribose 5-phosphate isomerase from the probiotic bacterium Lactobacillus salivarius UCC118. Acta Crystallogr Sect F Struct Biol Cryst Commun 68:1427–1433. https://doi.org/10.1107/S174430911204273X.
30. Zhao GX, Jin ZM, Wang YL, Allewell NM, Tuchman M, Shi DS. 2013. Structure and function of Escherichia coli RimK, an ATP-grasp fold, L-glutamyl ligase enzyme. Proteins 81:1847–1854. https://doi.org/10.1002/prot.24311.
31. Jiang WN, Hou Y, Inouye M. 1997. CspA, the major cold-shock protein of Escherichia coli, is an RNA chaperone. J Biol Chem 272:196–202. https://doi.org/10.1074/jbc.272.1.196.
32. Siguier P, Gourbeyre E, Chandler M. 2014. Bacterial insertion sequences: their genomic impact and diversity. FEMS Microbiol Rev 38:865–891. https://doi.org/10.1111/1574-6976.12067.
33. Hussain S, Devers-Lamrani M, Spor A, Rouard N, Porcherot M, Beguet J, Martin-Laurent F. 2013. Mapping field spatial distribution patterns of isoproturon-mineralizing activity over a three-year winter wheat/rape seed/barley rotation. Chemosphere 90:2499–2511. https://doi.org/10.1016/j.chemosphere.2012.10.080.
34. Sniegowski K, Bers K, Ryckeboer J, Jaeken P, Spanoghe P, Springael D. 2012. Minimal pesticide-primed soil inoculum density to secure maximum pesticide degradation efficiency in on-farm biopurification systems. Chemosphere 88:1114–1118. https://doi.org/10.1016/j.chemosphere.2012.04.057.
35. Sniegowski K, Bers K, Van Goetem K, Ryckeboer J, Jaeken P, Spanoghe P, Springael D. 2011. Improvement of pesticide mineralization in on-farm biopurification systems by bioaugmentation with pesticide-primed soil. FEMS Microbiol Ecol 76:64–73. https://doi.org/10.1111/j.1574-6941.2010.01031.x.
36. EFSA. 2015. Conclusion on the peer review of the pesticide risk assessment of the active substance isoproturon. EFSA J 13:4206. https://doi.org/10.2903/j.efsa.2015.4206.
37. Baelum J, Nicolaisen MH, Holben WE, Strobel BW, Sorensen J, Jacobsen CS. 2008. Direct analysis of tfdA gene expression by indigenous bacteria in phenoxy acid amended agricultural soil. ISME J 2:677–687. https://doi.org/10.1038/ismej.2008.21.
38. Martin-Laurent F, Piutti S, Hallet S, Wagschal I, Philippot L, Catroux G, Soulas G. 2003. Monitoring of atrazine treatment on soil bacterial, fungal and atrazine-degrading communities by quantitative competitive PCR. Pest Manag Sci 59:259–268. https://doi.org/10.1002/ps.630.
39. Jiang B, Jin NF, Xing Y, Su YP, Zhang DY. 2018. Unraveling uncultivable pesticide degraders via stable isotope probing (SIP). Crit Rev Biotechnol 38:1025–1048. https://doi.org/10.1080/07388551.2018.1427697.
40. Tsuda M, Minegishi K, Iino T. 1989. Toluene transposons Tn4651 and Tn4653 are class II transposons. J Bacteriol 171:1386–1393. https://doi.org/10.1128/jb.171.3.1386-1393.1989.
41. Gueguen E, Rousseau P, Duval-Valentin G, Chandler M. 2006. Truncated forms of IS911 transposase downregulate transposition. Mol Microbiol 62:1102–1116. https://doi.org/10.1111/j.1365-2958.2006.05424.x.
42. Tabata M, Ohhata S, Nikawadori Y, Kishida K, Sato T, Kawasumi T, Kato H, Ohtsubo Y, Tsuda M, Nagata Y. 2016. Comparison of the complete genome sequences of four gamma-hexachlorocyclohexane-degrading bacterial strains: insights into the evolution of bacteria able to degrade a recalcitrant man-made pesticide. DNA Res 23:581–599. https://doi.org/10.1093/dnares/dsw041.
43. Gai Z, Wang X, Liu X, Tai C, Tang H, He X, Wu G, Deng Z, Xu P. 2010. The genes coding for the conversion of carbazole to catechol are flanked by IS6100 elements in Sphingomonas sp. strain XLDN2-5. PLoS One 5:e10018. https://doi.org/10.1371/journal.pone.0010018.
44. Bignell C, Thomas CM. 2001. The bacterial ParA-ParB partitioning proteins. J Biotechnol 91:1–34. https://doi.org/10.1016/s0168-1656(01)00293-0.
45. Chen K, Xu X, Zhang L, Gou Z, Li S, Freilich S, Jiang J. 2016. Comparison of four Comamonas catabolic plasmids reveals the evolution of pBHB to catabolize haloaromatics. Appl Environ Microbiol 82:1401–1411. https://doi.org/10.1128/AEM.02930-15.
46. Maillard J, Regeard C, Holliger C. 2005. Isolation and characterization of Tn-Dha1, a transposon containing the tetrachloroethene reductive dehalogenase of Desulfitobacterium hafniense strain TCE1. Environ Microbiol 7:107–117. https://doi.org/10.1111/j.1462-2920.2004.00671.x.
47. Dziewit L, Baj J, Szuplewska M, Maj A, Tabin M, Czyzkowska A, Skrzypczyk G, Adamczuk M, Sitarek T, Stawinski P, Tudek A, Wanasz K, Wardal E, Piechucka E, Bartosik D. 2012. Insights into the transposable mobilome of Paracoccus spp. (Alphaproteobacteria). PLoS One 7:e32277. https://doi.org/10.1371/journal.pone.0032277.
48. Becker EC, Meyer RJ. 2002. MobA, the DNA strand transferase of plasmid R1162. The minimal domain required for DNA processing at the origin of transfer. J Biol Chem 277:14575–14580. https://doi.org/10.1074/jbc.M110759200.
49. Perruchon C, Vasileiadis S, Rousidou C, Papadopoulou ES, Tanou G, Samiotaki M, Garagounis C, Molassiotis A, Papadopoulou KK, Karpouzas DG. 2017. Metabolic pathway and cell adaptation mechanisms revealed through genomic, proteomic and transcription analysis of a Sphingomonas haloaromaticamans strain degrading orthophenylphenol. Sci Rep 7:6449. https://doi.org/10.1038/s41598-017-06727-6.
50. Nojiri H, Shintani M, Omori T. 2004. Divergence of mobile genetic elements involved in the distribution of xenobiotic-catabolic capacity. Appl Microbiol Biotechnol 64:154–174. https://doi.org/10.1007/s00253-003-1509-y.
51. Sun J-Q, Huang X, Chen Q-L, Liang B, Qiu J-G, Ali SW, Li S-P. 2009. Isolation and characterization of three Sphingobium sp. strains capable of degrading isoproturon and cloning of the catechol 1,2-dioxygenase gene from these strains. World J Microbiol Biotechnol 25:259–268. https://doi.org/10.1007/s11274-008-9888-y.
52. Aylward FO, McDonald BR, Adams SM, Valenzuela A, Schmidt RA, Goodwin LA, Woyke T, Currie CR, Suen G, Poulsen M. 2013. Comparison of 26 sphingomonad genomes reveals diverse environmental adaptations and biodegradative capabilities. Appl Environ Microbiol 79:3724–3733. https://doi.org/10.1128/AEM.00518-13.
53. Nielsen TK, Rasmussen M, Demaneche S, Cecillon S, Vogel TM, Hansen LH. 2017. Evolution of sphingomonad gene clusters related to pesticide catabolism revealed by genome sequence and mobilomics of Sphingobium herbicidovorans MH. Genome Biol Evol 9:2477–2490. https://doi.org/10.1093/gbe/evx185.
54. Stolz A. 2009. Molecular characteristics of xenobiotic-degrading sphingomonads. Appl Microbiol Biotechnol 81:793–811. https://doi.org/10.1007/s00253-008-1752-3.
55. Kostka JE, Green SJ, Rishishwar L, Prakash O, Katz LS, Marino-Ramirez L, Jordan IK, Munk C, Ivanova N, Mikhailova N, Watson DB, Brown SD, Palumbo AV, Brooks SC. 2012. Genome sequences for six Rhodanobacter strains, isolated from soils and the terrestrial subsurface, with variable denitrification capabilities. J Bacteriol 194:4461–4462. https://doi.org/10.1128/JB.00871-12.
56. Nalin R, Simonet P, Vogel TM, Normand P. 1999. Rhodanobacter lindaniclasticus gen. nov., sp, nov., a lindane-degrading bacterium. Int J Syst Bacteriol 49:19–23. https://doi.org/10.1099/00207713-49-1-19.

57. Hemme CL, Green SJ, Rishishwar L, Prakash O, Pettenato A, Chakraborty R, Deutschbauer AM, Van Nostrand JD, Wu L, He Z, Jordan IK, Hazen TC, Arkin AP, Kostka JE, Zhou J. 2016. Lateral gene transfer in a heavy metal-contaminated-groundwater microbial community. mBio 7:e02234-15. https://doi.org/10.1128/mBio.02234-15.
58. El-Sebai T, Lagacherie B, Cooper JF, Soulas G, Martin-Laurent F. 2005. Enhanced isoproturon mineralisation in a clay silt loam agricultural soil. Agron Sustain Dev 25:271–277. https://doi.org/10.1051/agro:2005003.
59. ISO. 2012. Soil quality—method to directly extract DNA from soil samples. ISO 11063. ISO, Geneva, Switzerland.
60. Martin-Laurent F, Philippot L, Hallet S, Chaussod R, Germon JC, Soulas G, Catroux G. 2001. DNA extraction from soils: old bias for new microbial diversity analysis methods. Appl Environ Microbiol 67:2354–2359. https://doi.org/10.1128/AEM.67.5.2354-2359.2001.
61. Zhou JZ, Bruns MA, Tiedje JM. 1996. DNA recovery from soils of diverse composition. Appl Environ Microbiol 62:316–322. https://doi.org/10.1128/AEM.62.2.316-322.1996.
62. Bru D, Martin-Laurent F, Philippot L. 2008. Quantification of the detrimental effect of a single primer-template mismatch by real-time PCR using the 16S rRNA gene as an example. Appl Environ Microbiol 74:1660–1663. https://doi.org/10.1128/AEM.02403-07.
63. ISO. 2016. Soil quality— estimation of abundance of selected microbial gene sequences by quantitative PCR from DNA directly extracted from soil. ISO 17601. ISO, Geneva, Switzerland.
64. Lopez-Gutierrez JC, Henry S, Hallet S, Martin-Laurent F, Catroux G, Philippot L. 2004. Quantification of a novel group of nitrate-reducing bacteria in the environment by real-time PCR. J Microbiol Methods 57:399–407. https://doi.org/10.1016/j.mimet.2004.02.009.
65. Zhang JJ, Kobert K, Flouri T, Stamatakis A. 2014. PEAR: a fast and accurate Illumina Paired-End reAd mergeR. Bioinformatics 30:614–620. https://doi.org/10.1093/bioinformatics/btt593.
66. Caporaso JG, Kuczynski J, Stombaugh J, Bittinger K, Bushman FD, Costello EK, Fierer N, Peña AG, Goodrich JK, Gordon JI, Huttley GA, Kelley ST, Knights D, Koenig JE, Ley RE, Lozupone CA, McDonald D, Muegge BD, Pirrung M, Reeder J, Sevinsky JR, Turnbaugh PJ, Walters WA, Widmann J, Yatsunenko T, Zaneveld J, Knight R. 2010. QIIME allows analysis of high-throughput community sequencing data. Nat Methods 7:335–336. https://doi.org/10.1038/nmeth.f.303.
67. Rognes T, Flouri T, Nichols B, Quince C, Mahe F. 2016. VSEARCH: a versatile open source tool for metagenomics. PeerJ 4:e2584. https://doi.org/10.7717/peerj.2584.
68. Caporaso JG, Bittinger K, Bushman FD, DeSantis TZ, Andersen GL, Knight R. 2010. PyNAST: a flexible tool for aligning sequences to a template alignment. Bioinformatics 26:266–267. https://doi.org/10.1093/bioinformatics/btp636.
69. Price MN, Dehal PS, Arkin AP. 2009. FastTree: computing large minimum evolution trees with profiles instead of a distance matrix. Mol Biol Evol 26:1641–1650. https://doi.org/10.1093/molbev/msp077.
70. Edgar RC. 2010. Search and clustering orders of magnitude faster than BLAST. Bioinformatics 26:2460–2461. https://doi.org/10.1093/bioinformatics/btq461.
71. McDonald D, Price MN, Goodrich J, Nawrocki EP, DeSantis TZ, Probst A, Andersen GL, Knight R, Hugenholtz P. 2012. An improved Greengenes taxonomy with explicit ranks for ecological and evolutionary analyses of bacteria and archaea. ISME J 6:610–618. https://doi.org/10.1038/ismej.2011.139.
72. Lozupone C, Knight R. 2005. UniFrac: a new phylogenetic method for comparing microbial communities. Appl Environ Microbiol 71:8228–8235. https://doi.org/10.1128/AEM.71.12.8228-8235.2005.
73. Andrews S. 2018. FastQC: a quality control tool for high throughput sequence data. http://www.bioinformatics.babraham.ac.uk/projects/fastqc.
74. Bolger AM, Lohse M, Usadel B. 2014. Trimmomatic: a flexible trimmer for Illumina sequence data. Bioinformatics 30:2114–2120. https://doi.org/10.1093/bioinformatics/btu170.
75. O'Connell J, Schulz-Trieglaff O, Carlson E, Hims MM, Gormley NA, Cox AJ. 2015. NxTrim: optimized trimming of Illumina mate pair reads. Bioinformatics 31:2035–2037. https://doi.org/10.1093/bioinformatics/btv057.
76. Butler J, MacCallum I, Kleber M, Shlyakhter IA, Belmonte MK, Lander ES, Nusbaum C, Jaffe DB. 2008. ALLPATHS: de novo assembly of whole-genome shotgun microreads. Genome Res 18:810–820. https://doi.org/10.1101/gr.7337908.
77. Okonechnikov K, Golosova O, Fursov M, UGENE Team. 2012. Unipro UGENE: a unified bioinformatics toolkit. Bioinformatics 28:1166–1167. https://doi.org/10.1093/bioinformatics/bts091.
78. Boetzer M, Henkel CV, Jansen HJ, Butler D, Pirovano W. 2011. Scaffolding pre-assembled contigs using SSPACE. Bioinformatics 27:578–579. https://doi.org/10.1093/bioinformatics/btq683.
79. Seemann T. 2014. Prokka: rapid prokaryotic genome annotation. Bioinformatics 30:2068–2069. https://doi.org/10.1093/bioinformatics/btu153.
80. Karsch-Mizrachi I, Takagi T, Cochrane G, International Nucleotide Sequence Database Collaboration. 2018. The International Nucleotide Sequence Database Collaboration. Nucleic Acids Res 46:D48–D51. https://doi.org/10.1093/nar/gkx1097.
81. Altschul SF, Gish W, Miller W, Myers EW, Lipman DJ. 1990. Basic local alignment search tool. J Mol Biol 215:403–410. https://doi.org/10.1016/S0022-2836(05)80360-2.
82. Guy L, Kultima JR, Andersson SGE. 2010. genoPlotR: comparative gene and genome visualization in R. Bioinformatics 26:2334–2335. https://doi.org/10.1093/bioinformatics/btq413.
83. R Core Team. 2017. R: a language and environment for statistical computing, reference index version 3.3.3. R Foundation for Statistical Computing, Vienna, Austria.
84. Huson DH, Auch AF, Qi J, Schuster SC. 2007. MEGAN analysis of metagenomic data. Genome Res 17:377–386. https://doi.org/10.1101/gr.5969107.
85. Xie Z, Tang H. 2017. ISEScan: automated identification of insertion sequence elements in prokaryotic genomes. Bioinformatics 33:3340–3347. https://doi.org/10.1093/bioinformatics/btx433.
86. Varani AM, Siguier P, Gourbeyre E, Charneau V, Chandler M. 2011. ISsaga is an ensemble of Web-based methods for high throughput identification and semi-automatic annotation of insertion sequences in prokaryotic genomes. Genome Biol 12:R30. https://doi.org/10.1186/gb-2011-12-3-r30.
87. Siguier P, Perochon J, Lestrade L, Mahillon J, Chandler M. 2006. ISfinder: the reference centre for bacterial insertion sequences. Nucleic Acids Res 34:D32–D36. https://doi.org/10.1093/nar/gkj014.
88. Robinson DG, Lee M-C, Marx CJ. 2012. OASIS: an automated program for global investigation of bacterial and archaeal insertion sequences. Nucleic Acids Res 40:e174. https://doi.org/10.1093/nar/gks778.